Impact of Porous-Media Topology on Turbulent Fluid Flow: Time-Resolved PIV Measurements

J. Härter[1,*], R. Poser[1], B. Weigand[1], G. Lamanna[1]

1: Institute of Aerospace Thermodynamics, University of Stuttgart, Germany
*Corresponding author: julian.haerter@itlr.uni-stuttgart.de

Keywords: PIV , Time-resolved PIV, TPMS, porous media, turbulent flow, interfacial region

ABSTRACT

An investigation of the interactions between a turbulent duct flow above a 3D porous medium with a periodic topology is reported. Both spatially and temporally resolved point measurements of velocity in the free flow and at the interface of the porous medium using the Particle Image Velocimetry (PIV) technique are presented. A Schwarz Primitive triply periodic minimal surface (TPMS) with a frequency of $f = \Pi/20$ printed from polyamide PA12 with a porosity of $\phi = 0.92$ was investigated as a porous structure. The periodicity of the model results in two different topologies, hill- and valley-alignment, each of which represent a measurement plane. These different alignments show a strong influence on the turbulent flow above the porous me dium. In addition to the time-averaged velocity field for the two alignments, velocity profiles as well as turbulent kinetic energy profiles at selected positions in flow direction are also shown. The influence of the turbulent channel flow on the porous model is shown by a contour plot of the time-resolved velocity, where this represents the turbulent fluctuation at a point in time. For the time-resolved plot, the same influence of the different topology to the respective alignments is s hown. With these time-resolved measurements, transient flow processes could be resolved, such as the detachment and attachment of the flow to the porous surface, which are also shown in this paper. These measurements provide an insight into the mechanism of energy, mass and momentum transfer at the interface between the free stream and the porous medium. The results presented are useful for further understanding of turbulent flows on flush mounted complex 3D structures and the influence of the periodic surface on the free flow.

1. Introduction

For the efficient design, operation and optimization of engineering applications such as transpiration cooling, filtration processes, heat exchangers, thermal insulation and geothermal engineering the influence of turbulent fluid flow interacting with different porous topologies need to be understood. Detailed and thorough knowledge of the interaction between the free stream and porous medium in terms of exchange of mass, momentum and energy are necessary for this purpose. A controversial point of discussion is whether transport at the interface is mainly controlled by diffusion or advection. The reason can be best understood by considering Fig. 1, where the influence

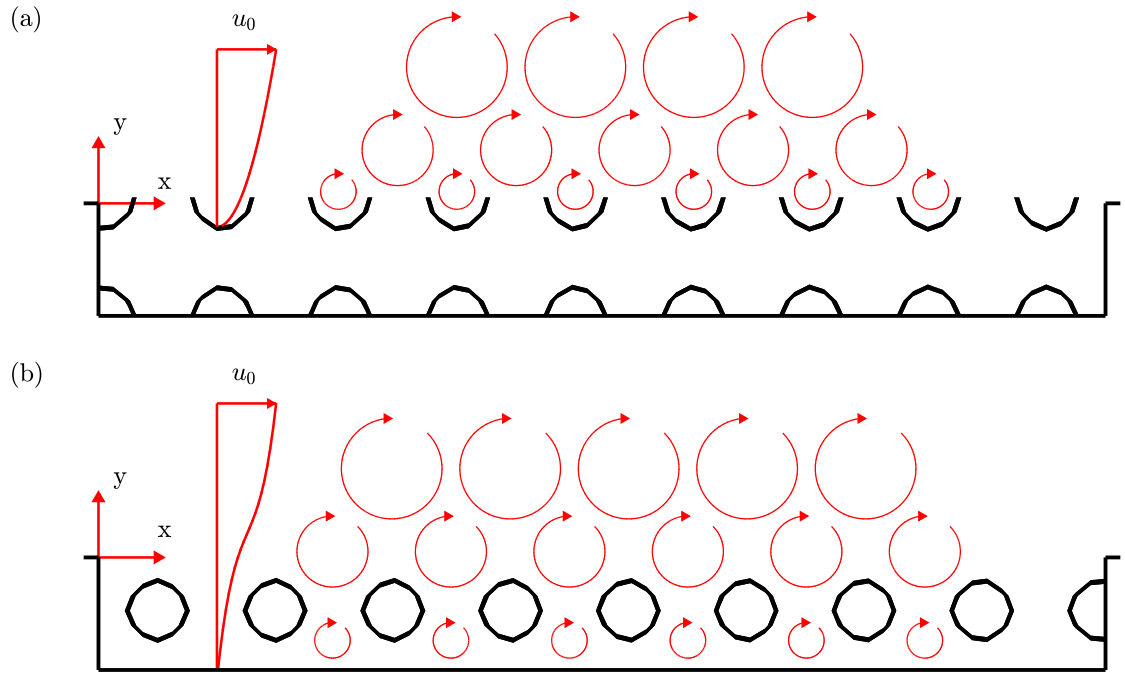

Figure 1. Sectional planes of a 3D porous medium with periodic topology: (a) diffusion-controlled, (b) turbulent interaction between free flow and porous medium region.

of the porous medium topology is crucial for the transport at the interface. Hahn et al. (2002) demonstrated that a viscous laminar sublayer exists close to the permeable wall only when $\sqrt{K}$ is small compared to the viscous length scale ν/u_τ. Here, K represents the intrinsic permeability of the porous medium, u_τ is the friction velocity at the permeable wall, and ν is the kinematic viscosity. With this requirement, Beavers & Joseph (1967) derived an empirical coupling condition for coupling the flow at the interface, where they assumed a direct proportionality between the strain rate at the interface and the velocity difference between the interfacial velocity u_s and the Darcy velocity u_D which was assumed in the porous domain, thus they made the assumption of very low flow velocities inside the porous medium. Breugem et al. (2006) added a permeability Reynolds number, definded by $Re_K = u_\tau\sqrt{K}/\nu$. When $Re_K \leq 1$, the discontinuous viscous sublayer over the wall elements combine to produce a continuous viscous sublayer ranging over the entire wall. However, as shown in Fig. 1 (a), larger interfacial velocities lead to the formation of bounded recirculation zones in the upper layer of the porous medium. In this latter case, it is not clear how to model the flow at the porous medium interface nor whether advection terms should be included in the coupling condition. For $Re_K > 1$, Suga et al. (2020) discovered that turbulent fluctuations begin to infiltrate the porous medium region, while the topology of the porous medium also influences turbulent flow in the free flow region. The relevance of Re_K was also confirmed by Manes et al. (2011). They reported that as the permeability increases, the near-wall structures of the turbulent flow change from coherent vortices to an unstable mixing layer caused by a Kelvin-Helmholtz instability in the mean shear rate. The challenge in these conditions is to determine the size of the prevailing eddies, which controls the size of the interfacial region. Between shear instability

and connected eddies, Manes et al. (2011) discovered two conflicting processes. Shear instability eddies get bigger and dominate momentum transmission at the interface as wall permeability and hence shear penetration increases.

The overall goal of this study is to experimentally investigate the exchange of momentum and energy for a 3D porous medium with periodic topology with a very high porosity and a small filament thickness. The complex porous 3D model under investigation is defined by two different topologies, as shown in Fig. 1, which influence the flow over it quite differently. Such anisotropic structures are expected to alter the flow both in the free flow and porous medium regions, in ways that are not fully understood. Therefore, we will focus on high resolved time and spatial measurements. This study describes a detailed method for time-resolved PIV measurements of a flush mounted 3D porous medium. The spatio-temporal properties of the fluid flow and the influence of the different topologies of the porous medium were investigated.

2. Experimental Methods and Procedures

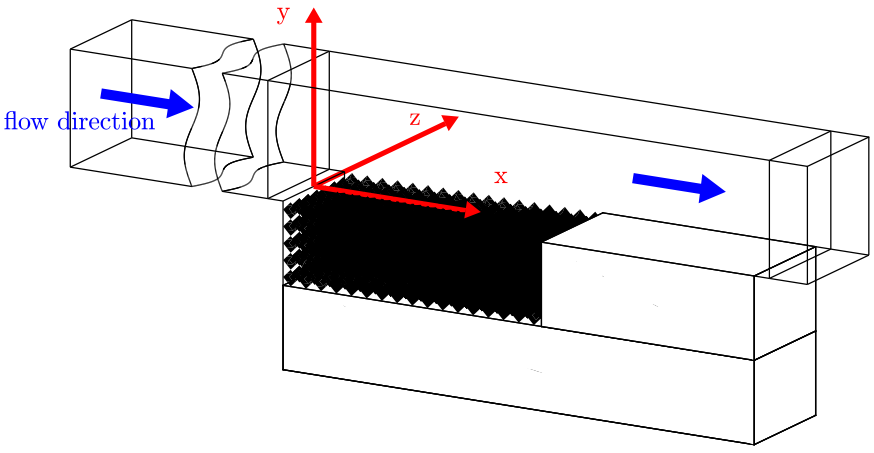

Figure 2. A schematic drawing of the test section.

A versatile facility was built to investigate enlarged models of 3D printed porous topologies. A schematic drawing of the test channel is shown in Fig. 2. The test rig design concept is modular, allowing the experimental investigation of different porous topologies and measurement techniques. The experimental setup is used to study the flow of a flush mounted porous media. The experiments were carried out in a square Plexiglas channel with a 0.34 m long test section located in a 6 m long wind tunnel. The test section consists of an upper square channel (0.14 m x 0.14 m x 0.34 m) and a lower reservoir (0.14 m x 0.1 m x 0.34 m) containing the porous medium. Upstream of the

test section, a 3 m long developing duct guides the airflow to the test section. The edge at the inlet duct to the cavity is the origin of the stream-wise direction $x = 0$ and the origin of the wall-normal direction $y = 0$ is placed at the interface between the free stream and the porous medium. The origin of the span-wise direction $z = 0$ is fixed at the symmetry plane of the channel. This leads to a right-handed Cartesian coordinate system with (x,y,z) denoting stream-wise, wall-normal and span-wise coordinate axes.

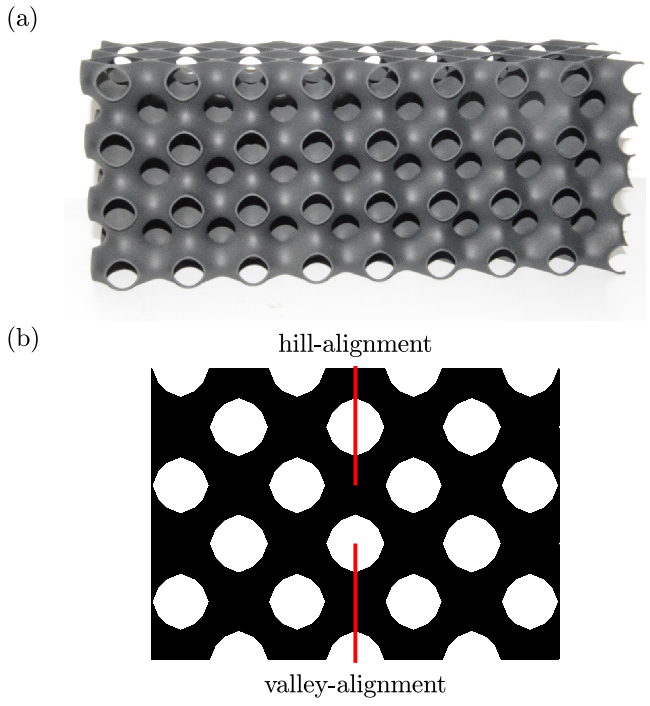

Figure 3. (a) Picture of the porous medium, (b) Cross section of the porous medium.

The investigated porous 3D model was fabricated using Multi Jet Fusion (MJF) by Rapidobject GmbH, which is similar to selective laser sintering. The material used was polyamide PA12. The triply periodic minimal surface (TPMS) which was selected as the porous topology to be investigated is a Schwarz Primitive ('Schwarz P'). This P surface can be approximated by Eq. 1, which defines the surface dividing a volume where x, y and z are the Cartesian coordinates.

$$cos(xf) + cos(yf) + cos(zf) = 0 \tag{1}$$

The surface divides the volume equally, and it can be printed as a solid phase at all points where Eq. 1 is valid. To create such a three-dimensional model the primary equation of Schwarz was supplemented with a frequency f to achieve the a geometry with dimensions of 140 x 100 x 340 mm. The wall thickness of this surface was set up to 1 mm. Thus, the porosity of the studied model is approximately $\phi = 0.92$, which is given by the frequency $f = \Pi/20$. With this frequency and the given height of the model two different topologies of the measurement region occur, and a wavelength of periodicity of the model of $\lambda_{\mathrm{pm}} = 40$ mm. Figure 3 shows the cross section of the porous medium and the measurement plane of the two different topologies referred as hill- and valley-alignment.

Dry air is used as the working fluid. Oil droplets with a mean diameter of 0.1 to 1 μm were injected into the free stream. By changing the pressure on the particle generator, the amount of oil droplets could be adjusted. The Reynolds number of the channel flow was calculated by:

$$Re = \frac{\dot{m}}{\mu H} \tag{2}$$

based on the channel height H and the mass flow rate $\dot{m}$ of the inlet duct. Thus, measurements were performed at four different Reynolds numbers. This represents a global Reynolds number of the duct flow, local Reynolds numbers inside the porous medium differ from this global Reynolds number, due to significantly lower characteristic velocities and reduced hydraulic diameter.

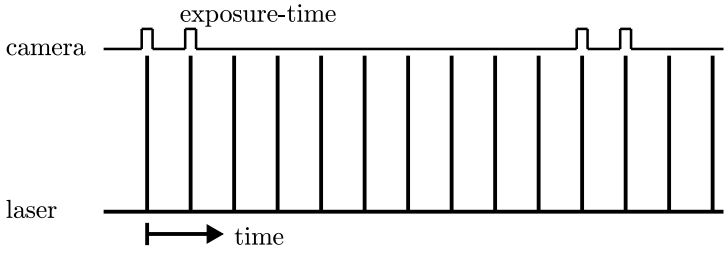

Figure 4. Recording mode for cyclic time based time-resolved PIV.

To obtain quantitative information about the dynamic process at the interfacial region, time-resolved 2D2C PIV measurements were performed in the test facility. A single cavity high-speed laser supplied by Edgewave with a maximum pulse repetition rate of 10 kHz and a 532 nm wavelength was used to illuminate a plane within the test section. A Nikkor lens (F = 50 mm) is fitted to a Photron Fastcam SA-X2 which is used to capture images. For the selected porous media model nine different positions covering the whole interfacial region in stream-wise direction were captured. Each single field of view is approximately 80 mm x 80 mm with a resolution of 1024 x 1024 pixel. To fulfil the general PIV requirements of two images of illuminated particles with a time interval to allow the determination of the particle image displacement, the laser pulse rate was set between 4 kHz and 10 kHz depending on the free stream Reynolds number. However, this leads to the fact that only very short time periods can be recorded and thus large-scale frequency phenomena can not be investigated. To solve this limitation of the recording time, a cycle time based recording mode, which is shown in Fig. 4 , was used. The cyclic time based measurement is designed for periodic event recordings. While the laser illuminates the flow with a frequency of e.g. 5 kHz, the camera captures only one image pair every 500 Hz. The repetition rate between every two image pairs can be chosen such that the flow phenomena of interest are properly sampled, but the acquisition is still time-resolved. Each recording consists of 4000 single frames at every single positions, which are than combined into 2000 double frame images. The commercial software Davis 10.2 is used to operate the PIV system, and to process data that was acquired. The time-resolved images are post-processed, with a multi-pass FFT cross-correlation algorithm to determine the average displacement within the interrogation area. For conducting the PIV evaluation decreasingly smaller

window sizes of interrogation areas are used. The evaluation starts with the first pass with the initial interrogation areas of 64 x 64 pixel and 50 % overlap. In the next pass the window size is decreased to 16 x 16 pixel and the vector calculated in the first pass is used as a best-choice window shift. In this manner the window shift is adaptively improved to compute the vectors in the following steps more accurately and more reliably. The decreasing window size allows to use a much smaller final interrogation area than it would be possible without adaptive window shifting. This improves the spatial resolution of the vector field and produces less erroneous vectors.

3. Results and Discussion

The averaged vector field were determined from the 2000 double frame images for each position and then compiled into one data set of the whole interface. By means of this averaging, statistical uncertainties and the effect of spurious vectors are reduced. Vector fields of the instantaneous velocity will be discussed later. In Fig. 5 the time-averaged mean velocity field $|V|$ normalized by the centerline velocity of the free stream is shown for the hill- and valley-alignment. The main flow direction is from left to right. The x-direction distance is non-dimensionalized by the wavelength of one period and the y-direction by the hydrodynamic boundary layer thickness of the free flow for a fully developed duct flow, respectively.

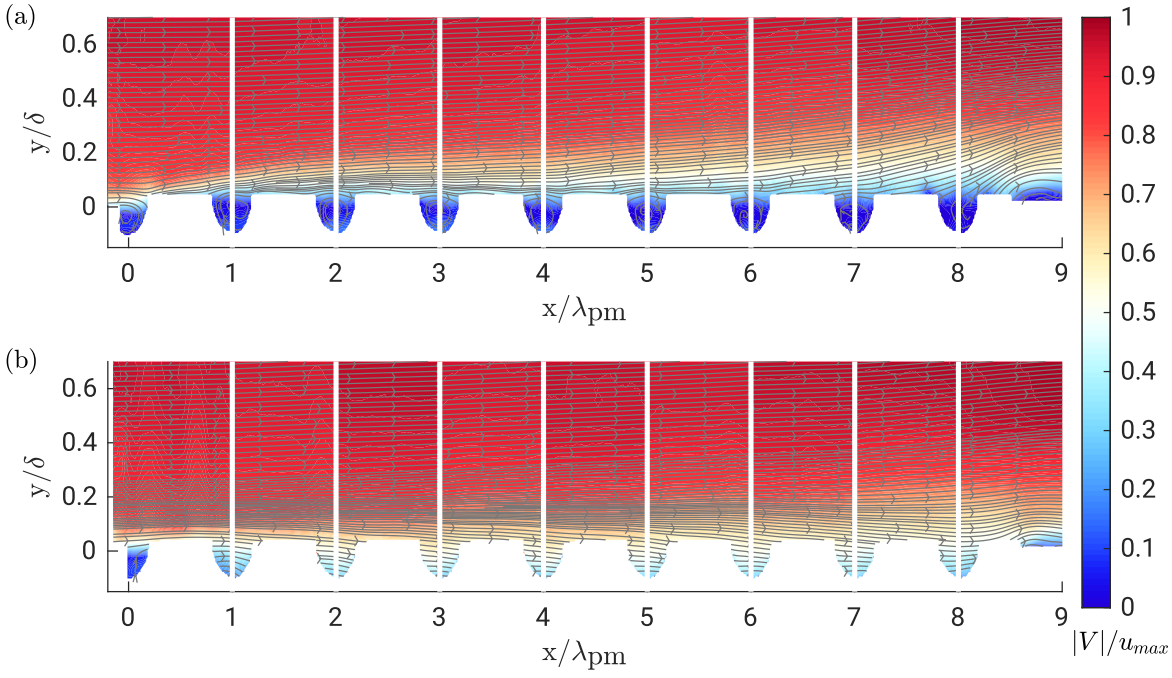

Figure 5. Time averaged $|V|$-velocity contour plot normalized by the centerline velocity at $Re = 21{,}300$: (a) hill-alignment, (b) valley-alignment.

At the interface between the free flow and the porous medium, the no slip condition is no longer satisfied and an exchange of mass, momentum and energy can be observed. The different influ-

ences of the topology of the porous medium alignment on the overlying flow can be clearly seen. For the hill-alignment of the porous medium, shown in Fig. 5 (a), an increase in the boundary layer thickness along the entire length of the porous model and a strong outflow at the end can be seen. The formation of small vortices in the holes of the surface are also significant in this alignment, creating a shear layer in the interfacial region. The boundary layer formation for the case of the valley-alignment, shown in Fig. 5 (b), is significantly smaller. Here, the streamlines do not indicate any vortices on the surface of the porous structure. The velocities at the wall of the porous medium, so called interfacial velocity, is significantly higher for this case.

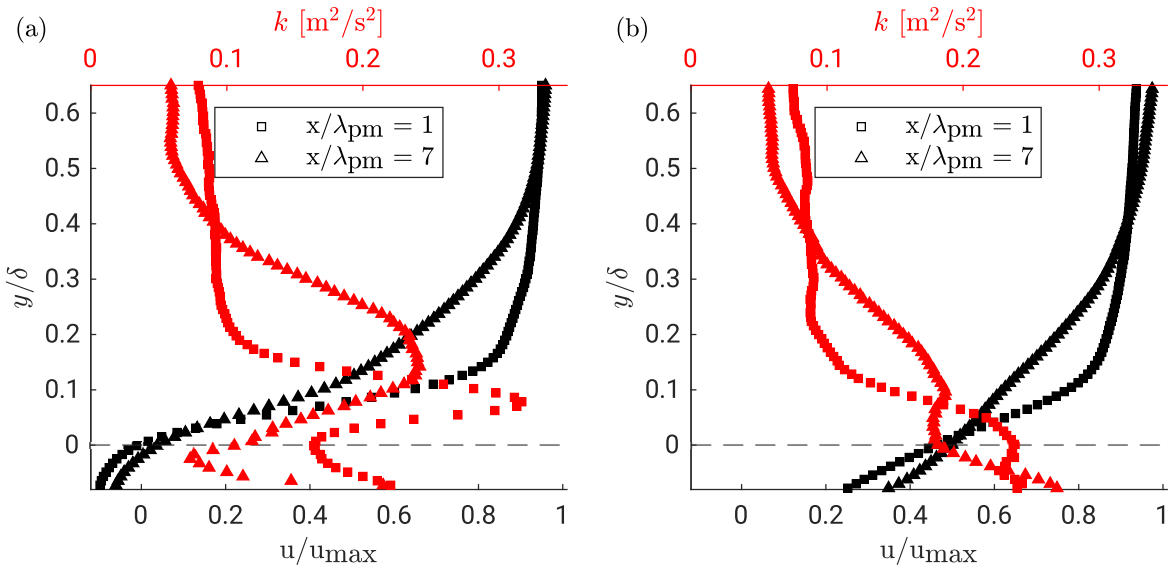

Figure 6. Time averaged velocity u and turbulent kinetic energy profiles at different x positions for $Re = 21{,}300$: (a) hill-alignment, (b) valley-alignment.

By measuring detail velocity data at the interface better insights into the hydrodynamic coupling at the interface can be obtained. Figure 6 shows the time-averaged velocity profiles and turbulent kinetic energy profiles at two different stream-wise positions above the porous medium for the hill- and valley-alignment at a free stream Reynolds number of $Re = 21{,}300$. As previously stated, the increase of the boundary layer thickness for the hill-alignment case can be observed. The turbulent kinetic energy is a measure of the turbulence intensity. For the hill-alignment in Fig. 6 (a) the profiles of the turbulent kinetic energy show a region of intense turbulence generation above the porous medium due to shearing between the high momentum free flow and the low momentum flow inside the porous medium. While the thickness of the region with higher turbulent kinetic energy is initially smaller and has a higher peak value, as the flow direction increases the peak value becomes smaller and the thickness of the turbulent kinetic energy layer increases. In the porous medium, the amount of the turbulent kinetic energy increases for both flow positions, but is significantly lower as in the free stream.

For the valley-alignment in Fig. 6 (b), a similar behavior is seen for the kinetic energy profiles. With increasing length of the porous model, the turbulent kinetic energy layer rises to higher y-

values. Also, the thickness of the turbulent kinetic energy layer at the beginning of the porous medium is thinner than at the end. Since the valley-alignment does not show such a strong shear layer as in the hill-alignment, the values of the turbulent kinetic energy are lower right above the porous medium. For larger y-values, both alignments show comparable values of the turbulent kinetic energy in the free stream flow. Also for this alignment, the values within the porous model increase and have their maximum there.

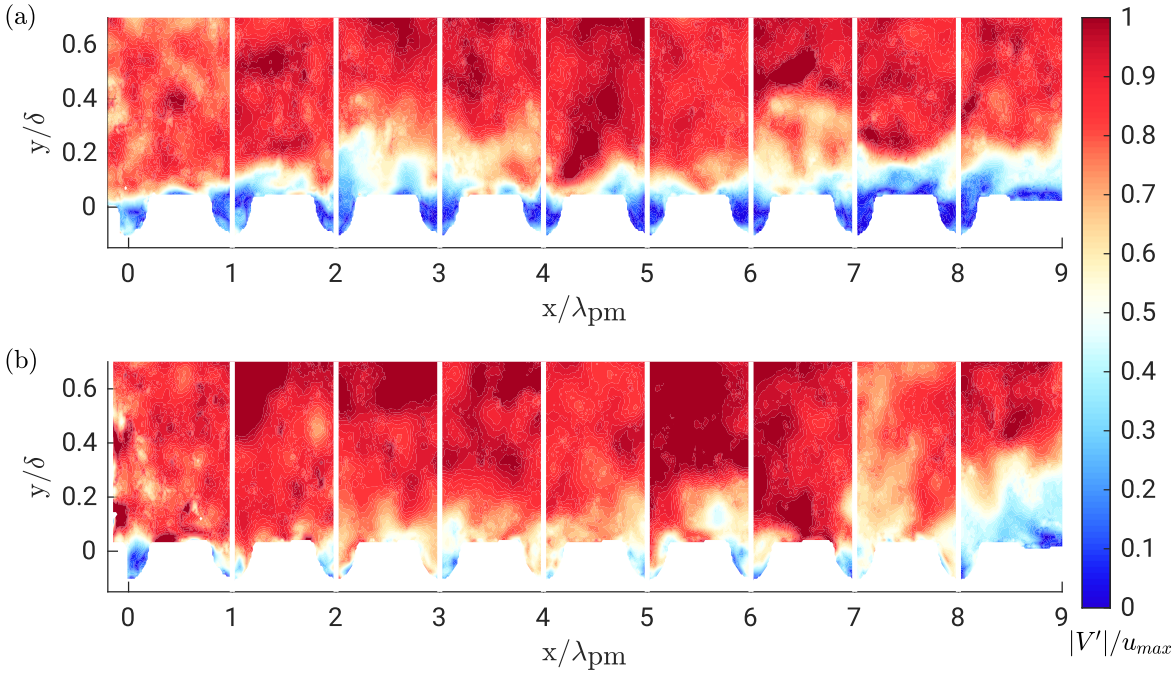

Figure 7. Instantaneous $|V'|$-velocity contour plot normalized by the centerline velocity at $Re = 21{,}300$: (a) hill-alignment, (b) valley-alignment.

The time-resolved PIV technique offers the possibility to analyse the development of turbulence in detail and to achieve temporal information about the flow field. The timescales of interest are much smaller than they could be resolved with a standard 2D2C PIV approach, which are typically a few Hertz. The temporal resolution allows one to see the differences from the individual instantaneous image acquired. In Fig. 7 the normalized velocity magnitude of one snapshot is shown. Due to the different recording times between the individual positions, the instantaneous velocity field does not give a uniform statement about the different recorded positions. Nevertheless, similar findings can be derived about the flow field at the interface in comparison to the averaged measurements. As in Fig. 5 the different alignments of the porous medium are shown here. For the hill-alignment there are regions of low velocities at the interface, probably caused by the high shear rate of this topology. These separation regions of the flow are clearly visible for the hill-alignment in Fig. 7 (a). As for the time-averaged contour plots, here the significant increase of the interfacial velocity for the valley-alignment can be observed. With this time resolution, a temporal analysis on the velocity development and the turbulence can be made for each individual position. This clearly shows the influence of the turbulent free flow on the exchange of the mass and momentum in the interfacial

region.

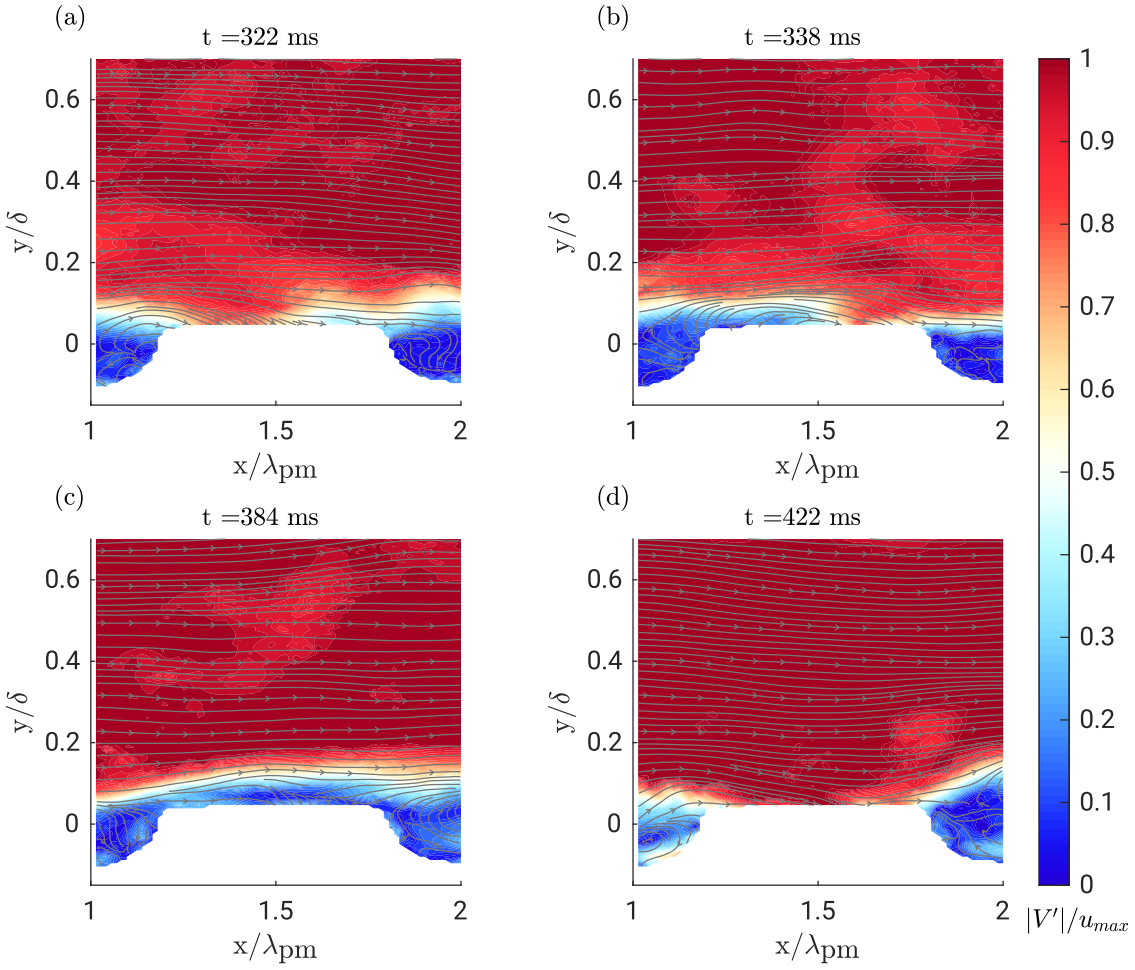

Figure 8. Instantaneous $|V'|$-velocity contour plot normalized by the centerline velocity of the hill-alignment at $Re = 8{,}500$: (a) $t = 322$ ms, (b) $t = 338$ ms, (c) $t = 384$ ms, (d) $t = 422$ ms.

Individual detailed images of these instantaneous velocity fields show that certain phenomena occur over the duration of a measurement at certain frequencies. Such a time-frequency dependent characteristic for the hill-alignment can be seen in Fig. 8. Here, the normalized velocity magnitude fluctuations by the averaged centerline velocity are shown for selected time steps. Due to these different time steps, a non-stationary behavior of the flow at the interface of the porous medium is observed. The position shown is at the beginning of the porous medium from $1 \leq x/\lambda_{\mathrm{pm}} \leq 2$. For the first time step at 322 ms the high velocity free flow is attached to the hill, which is in between the two holes given by the topology of the hill-alignment. These holes show the typically low velocity regions for this alignment, as already discussed. These low velocities expand to the next time step and begin to form a low velocity region over the hill. But, a part of the surface at the interface of the hill still have higher velocities. This region of higher velocity then completely detaches from the hill at time step 384 ms. Here, a total flow around the hill with low interface velocities is seen. This flow process then continues for a time before the higher velocities reattach to the model surface

and form a region of higher velocity over the hill. Finally, this leads back to the initial time step, where the velocity at the interface is high over the hill and low in the surrounding valleys. With the time-resolved data more of these detachments and attachments could be observed. Further investigations will focus on these frequencies and the temporal behavior of this porous model.

4. Conclusions

Knowledge of the flow over and through porous media is necessary for an accurate prediction of the flow rate, the momentum transfer, and the design of efficient engineering systems. Experimental data are therefore crucial to develop modeling concepts capable to reproduce these phenomena. In this study, we presented for the first time a detailed time-resolved analysis of pressure driven flow over a periodic 3D porous medium under turbulent boundary conditions. It was demonstrated that, depending on their alignment, different flow conditions result for such a periodic 3D structure. The results clearly show the influence of turbulent flow on the flush-mounted porous medium and the demand for time-resolved measurement and visualization of such flow phenomena.

Future investigations will focus on the understanding of the dynamic processes at the interface leading to the enhancement of turbulence in the near-wall region of the free flow. For this purpose, measurements with more images must be performed in order to be able to resolve the turbulent fluctuations even better. This will not be possible with the current setup, since the measurement time is limited by the thermal power on the surface of the model. Thus, the influence of the topology on the turbulence development in the free stream and the porous medium will be further investigated. Other alignments or planes of the porous medium will also be measured to learn even more about the influence of the periodicity of this structure. Furthermore, frequency analyses will provide further understanding of transport phenomena at the interface to the porous medium.

Acknowledgements

The authors gratefully acknowledge the support of the DFG for this project.
Funded by Deutsche Forschunggemeinschaft (DFG, German Research Foundation) under Germany's Excellence Strategy - EXC 2075 - 390740016.
Funded by the Deutsche Forschungsgemeinschaft (DFG, German Research Foundation) – Project Number 327154368 – SFB 1313.
We are also grateful for the support in the project GZ 1577, funded by the DFG.

Nomenclature

F	Focal length [m]
f	Frequency [1/s]
H	Channel height [m]
k	Turbulent kinetic energy [m^2/s^2]
K	Permability [m^2]
$\dot{m}$	Mass flow rate [kg/s]
Re	Reynolds number [-]
Re_K	Permeability Reynolds number [-]
t	Time [s]
u	Stream-wise velocity [m/s]
u_0	Free stream velocity [m/s]
u_D	Darcy velcoity [m/s]
$u_{\max}$	Centerline velocity [m/s]
u_τ	Friction velocity [m/s]
V	Mean velocity [m/s]
V'	Fluctuating mean velocity [m/s]
x	Stream-wise direction [m]
y	Wall-normal direction [m]
z	Span-wise direction [m]
δ	Boundary layer thickness [m]
λ_{pm}	Wavelength of periodicity [m]
μ	Dynamic viscosity [Pa s]
ν	Kinematic viscosity [m^2/s]
ϕ	Porosity [-]

References

Beavers, G. S., & Joseph, D. D. (1967). Boundary conditions at a naturally permeable wall. *Journal of Fluid Mechanics*, *30*(1), 197–207. doi:

Breugem, W. P., Boersma, B. J., & Uittenbogaard, R. E. (2006). The influence of wall permeability on turbulent channel flow. *Journal of Fluid Mechanics*, *562*, 35–72. doi:

Hahn, S., Je, J., & Choi, H. (2002). Direct numerical simulation of turbulent channel flow with permeable walls. *Journal of Fluid Mechanics*, *450*, 259–285. doi:

Manes, C., Poggi, D., & Ridolfi, L. (2011, 11). Turbulent boundary layers over permeable walls: Scaling and near-wall structure. *Journal of Fluid Mechanics*, *687*, 141 - 170. doi:

Suga, K., Okazaki, Y., & Kuwata, Y. (2020, 02). Characteristics of turbulent square duct flows over porous media. *Journal of Fluid Mechanics*, *884*. doi: